Robust quantum boomerang effect in non-Hermitian systems

Flavio Noronha [1,2] José A. S. Lourenço [1] and Tommaso Macrì [1,3]

[1]*Departamento de Física Teórica e Experimental, Universidade Federal do Rio Grande do Norte, Campus Universitário, Lagoa Nova, Natal-RN 59078-970, Brazil*

[2]*Institute for Theoretical Physics, Utrecht University, Princetonplein 5, 3584 CC Utrecht, Netherlands*

[3]*ITAMP, Harvard-Smithsonian Center for Astrophysics, Cambridge, Massachusetts 02138, USA*

(Received 24 June 2022; revised 13 September 2022; accepted 20 September 2022; published 29 September 2022)

Anderson localization is a general phenomenon that applies to a variety of disordered physical systems. Recently, a manifestation of Anderson localization for wave packets launched with a finite average velocity was proposed, the quantum boomerang effect (QBE). This phenomenon predicts that the disorder-averaged center of mass of a particle initially moves ballistically, then makes a U-turn, and finally slowly returns to its initial position. The QBE has been predicted to take place in several Hermitian models with Anderson localization and has been experimentally observed in the paradigmatic quantum kicked rotor model. In this paper, we investigate the emergence of the QBE in non-Hermitian systems and clarify the importance of symmetries of the Hamiltonian and the initial state. We generalize the analytical arguments available in the literature and show that even in the case of complex spectrum a boomeranglike behavior can appear in a non-Hermitian system. We confirm our analytical results through a careful numerical investigation of the dynamics for several non-Hermitian models. We find that non-Hermiticity leads to the breakdown of the dynamical relation, though the QBE is preserved. This paper opens avenues for future investigations in Anderson localized systems. The models studied here may be implemented using cold atoms in optical lattices.

DOI: 10.1103/PhysRevB.106.104310

I. INTRODUCTION

It is well-known that a propagating wave in a disordered or random environment is subject to multiple scatterings and may lead to destructive self-interference. This interference is the cause of several phenomena in nature, including the Anderson localization (AL) of quantum particles, i.e., the absence of wave diffusion in disordered potentials [1]. AL has been experimentally observed in many platforms, including light [2,3], ultrasound waves [4], and atomic matter [5–9]. AL is not restricted to Hermitian models. There are several non-Hermitian models in which the disorder leads to this localization, including, e.g., models with asymmetric hopping [10–31] and models with gain and loss parameters, i.e., complex on-site potentials [32–38], that can be experimentally implemented with several platforms [23,39,40].

Interesting transitions can appear in non-Hermitian systems as one changes the parameters of the model. These include not only the Anderson transition but also topological transitions [31,40,41] and transitions from a phase with complex eigenenergies to a phase where all eigenenergies are real, called real-complex transitions. The real-complex transitions usually occur in, but are not restricted to, models with parity-time (PT) symmetry [41–51] and models with time-reversal (T) symmetry [26,52].

The non-Hermitian Hatano-Nelson (HN) and Hermitian Aubry-André (AA) models are paradigmatic examples showing AL transitions. The HN model describes a disordered system with asymmetric hoppings [10]. Interestingly, the three transitions (the Anderson, topological, and real-complex transitions) take place simultaneously in the HN model with periodic boundary conditions (PBCs). As one increases the non-Hermiticity in that model, the system moves from a phase with all states localized, all eigenenergies real, and a trivial topological number to a phase with some extended states, complex eigenenergies, and a nontrivial topological number [26,27]. The AA model is a well-known Hermitian model with pseudorandom potential which possesses a mobility edge [53,54]. There are several non-Hermitian generalizations of the AA model which also display localization transitions [24,29,41,52,55]. In Ref. [31], the authors investigated a PT-symmetric non-Hermitian AA model and found three distinct phases. In the PT-broken phase, the system presents complex eigenenergies and extended states. There are two PT-unbroken phases in the model. In one of them, there are extended states while in the other one all states are localized.

AL has direct implications for the transport properties of disordered materials. A genuine dynamical phenomenon due to AL, called quantum boomerang effect (QBE) has been recently introduced in Ref. [56]. To explain the QBE, it is pertinent to recall the behavior of a traditional boomerang. Releasing a boomerang with an initial velocity, the boomerang will initially move away from its origin and, after some time, return to its initial position. Analogously, in the quantum realm, releasing a particle launched with momentum k_0 in a T-symmetric disordered potential leads to the QBE: The disorder-averaged center of mass (DACM) of the particle $\overline{\langle x(t)\rangle}$ initially moves balistically, departs from the origin [i.e., $\overline{\langle x(t)\rangle} \approx v_0 t$ for $t \ll \tau$, where τ is the mean free time], then makes a U-turn and slowly returns to its initial position,

$\overline{\langle x(+\infty)\rangle} = 0$ [56]. Here $\overline{(\cdots)}$ denotes disorder average, $\langle\cdots\rangle$ is the expectation value of an observable and v_0 is the initial velocity of the wave packet. In practice, when the QBE is present one can observe $\overline{\langle x(t)\rangle} \approx 0$ at finite times (if $t \gg \tau$) even in the limit of large system sizes. This intriguing quantum phenomenon is different from the behavior expected for the classical disordered counterpart, where the center of mass would initially move away from the origin and saturate at an approximate distance ℓ from the starting point, where ℓ is the mean-free path [56]. The QBE was predicted to occur in several models with AL [57]. Most of the models satisfy the dynamical relation [56,57]

$$\frac{d}{dt}\overline{\langle x^2(t)\rangle} = 2v_0\overline{\langle x(t)\rangle}, \tag{1}$$

which shows that the DACM is connected to the spreading of the wave packet. According to it, $\overline{\langle x(t)\rangle}$ can only come back to the origin when the wave function stops spreading. Recently, the QBE was verified in an experimental realization of the quantum kicked rotor [58].

All previous results on the QBE were found in Hermitian T-symmetric systems and several questions arose concerning which are the most general initial conditions and properties of the model required for the QBE to exist. Very recently, two independent works established that T symmetry of the Hamiltonian is not fundamental to observe the QBE and showed sufficient conditions to observe the effect [59,60]. Though Ref. [60] focused on Hermitian models, the presented analytical arguments predict the QBE in both Hermitian and non-Hermitian systems with real spectrums.

In the present paper, we numerically confirm the presence of the QBE in several non-Hermitian models, establishing that Hermiticity is not a necessary condition for the QBE to exist. Here we also investigate the main characteristics of this effect in non-Hermitian systems and show models where the QBE is not observed. We focus on general one-dimensional disordered lattice models which display AL. We study their dynamics employing extensive numerical simulations.

We briefly summarize the main findings and the structure of the paper. In Sec. II, we review and generalize the analytical arguments that lead us to expect a boomerang behavior in both Hermitian and non-Hermitian systems. In Sec. III, we discuss numerical results showing the QBE in the HN model and in a random-hopping model, which are non-Hermitian models with T symmetry. If the model is T symmetric, a boomeranglike behavior can be present even in the case of complex eigenenergies. We also show the presence of the QBE in the Hermitian AA model and in its non-Hermitian PT-symmetric generalization. The QBE is also shown in a non-Hermitian random hopping model with disorder in the complex phase of the hopping. This model is more general than all other models considered in the literature about QBE in the sense that it simultaneously breaks Hermiticity, T, P, and PT symmetries. Investigating other models without T or PT symmetry in phases with AL and complex spectra, we find that the DACM, instead of reaching the origin, typically presents a local minimum after the U-turn, and then increases again. This is the case of, e.g., the HN model with complex potential, the Anderson model with alternating gain and loss with constant magnitude, and a random gain and loss model. In Sec. IV, we summarize our findings, mention possible experimental realizations of some non-Hermitian models and provide interesting scenarios to generalize this work. Finally, in the Appendix we discuss some details regarding the saturation of the variance when the QBE is present and the breakdown of the dynamical relation in the non-Hermitian models considered here.

II. DERIVATION OF THE QBE

In this section, we provide a review of the analytical arguments with sufficient conditions for the existence of the QBE in non-Hermitian models, as discussed in Ref. [60], and extend the discussion for the boomeranglike behavior in the case of complex eigenenergies. We focus on the symmetries of the initial state and the disordered non-Hermitian Hamiltonian. For compactness of notation, we discuss one-dimensional models. However, all the considerations below can be immediately generalized to an arbitrary number of spatial dimensions. The boomerang effect is expected to appear if (a) the Hamiltonian presents AL; (b) the spectrum is real or, in the case of complex spectrum, the Hamiltonian H is T symmetric; (c) the ensemble $\{H\}$ of all disorder realizations of the model is PT invariant, $PT\{H\}(PT)^{-1} = \{H\}$, i.e., for each disorder realization H, its parity-time counterpart $\tilde{H} = PTH(PT)^{-1}$ is also a disorder realization of the same model; and (d) the initial state is an eigenstate of PT, $PT|\psi_0\rangle = \pm|\psi_0\rangle$ [60]. Here T is the time-reversal operator and P is the spatial inversion operator.

To demonstrate the presence of the boomerang effect with the previous conditions, in the following we write expressions for the center of mass $\langle x(t)\rangle$. We divide the demonstration in the two different cases of condition (b). In the case where all eigenvalues are real, expanding $|\psi_0\rangle = \sum_n c_n|\phi_n\rangle$ in terms of the eigenvectors of the Hamiltonian, $H|\phi_n\rangle = \epsilon_n|\phi_n\rangle$, using condition (a), taking the average over disorder realizations and taking the limit $\overline{\langle x(+\infty)\rangle} := \lim_{t\to+\infty}\overline{\langle x(t)\rangle}$, one finds the diagonal ensemble [56,58–61]

$$\overline{\langle x(+\infty)\rangle} = \overline{\sum_n |\psi_0\phi_n|^2\langle\phi_n|X|\phi_n\rangle}, \tag{2}$$

where X is the position operator. This diagonal ensemble is a good approximation at finite times (if $t \gg \tau$) even in the limit of large system sizes. Following similar steps, we find the same expression for $\overline{\langle x(-\infty)\rangle}$ and then

$$\overline{\langle x(+\infty)\rangle} = \overline{\langle x(-\infty)\rangle}. \tag{3}$$

Equations (2) and (3) are valid for real spectrum. Now we consider the case of complex eigenenergies. Let $|\phi_l\rangle$ be the eigenstate with finite overlap with $|\psi_0\rangle$ ($\langle\phi_l||\psi_0\rangle \neq 0$), which has the largest value for the imaginary part of its eigenvalue, i.e., $\varepsilon_n'' < \varepsilon_l''$, $\forall n$. Similarly, let $|\phi_m\rangle$ be the eigenstate which has the smallest value for the imaginary part of its eigenvalue, i.e., $\varepsilon_m'' < \varepsilon_n''$, $\forall n$. For simplicity, we assume that ϵ_l'' and ϵ_m'' are nondegenerate. Once there are complex eigenenergies, the time evolution of the wave function is not norm preserving. The center of mass is given by $\langle x(t)\rangle = \langle\psi(t)|X|\psi(t)\rangle/\langle\psi(t)|\psi(t)\rangle$, where $|\psi(t)\rangle = \exp(-iHt)|\psi_0\rangle$ and $\langle\psi(t)| = \langle\psi_0|\exp(+iH^\dagger t)$. Inserting the identity

$I = \sum |\phi_n\rangle\langle\phi_n|$ in the expression for $\langle x(t)\rangle$ and using the previous relations we find, for $t \to +\infty$ and $t \to -\infty$,

$$\langle x(+\infty)\rangle = \langle\phi_l| X |\phi_l\rangle, \tag{4}$$

$$\langle x(-\infty)\rangle = \langle\phi_m| X |\phi_m\rangle. \tag{5}$$

We recall that if the Hamiltonian is T (or PT) symmetric and has a complex eigenvalue ε, then ε^* is also an eigenvalue. Indeed, if $K = T$ (or $K = PT$) and $|\phi\rangle$ is an eigenvector of H, then

$$\begin{aligned} H|\phi\rangle &= \varepsilon|\phi\rangle, \\ KH|\phi\rangle &= H(K|\phi\rangle) = K\varepsilon|\phi\rangle = \varepsilon^*(K|\phi\rangle), \end{aligned} \tag{6}$$

and $K|\phi\rangle$ is the associated eigenvector. For a T-symmetric H, we use the property above to find $\varepsilon_m = \varepsilon_l^*$, $|\phi_m\rangle = T|\phi_l\rangle$ and $\phi_m(x) = \phi_l^*(x)$, where $\phi_m(x) = \langle x|\phi_m\rangle$ and $\phi_l(x) = \langle x|\phi_l\rangle$. Therefore, even in the case with complex spectrum, if the Hamiltonian is T symmetric [i.e., condition (b)], we have from Eqs. (4) and (5) $\langle x(+\infty)\rangle = \langle x(-\infty)\rangle$, and hence Eq. (3). For a Hamiltonian H with PT symmetry (without T symmetry), we do not obtain Eq. (3) because, using the properties above, we get $|\phi_m\rangle = PT|\phi_l\rangle$, $\phi_m(x) = \phi_l^*(-x)$ and hence $\langle x(+\infty)\rangle = -\langle x(-\infty)\rangle$.

Now, we assume condition (c) without requiring H to be T or PT symmetric. Therefore, for each disorder realization H, its parity-time counterpart $\tilde{H} = PTH(PT)^{-1}$ is also a disorder realization of the same model. Then, inserting $(PT)^{-1}PT$ in the expression for $\langle x(t)\rangle$, we find

$$\begin{aligned} \langle x(t)\rangle_H &= \frac{\langle\psi_0|\exp(+iH^\dagger t)\, X \exp(-iHt)|\psi_0\rangle}{\langle\psi_0|\exp(+iH^\dagger t)\exp(-iHt)|\psi_0\rangle} \\ &= \frac{\langle\psi_0|\exp(-i\tilde{H}^\dagger t)(-X)\exp(i\tilde{H}t)|\psi_0\rangle}{\langle\psi_0|\exp(-i\tilde{H}^\dagger t)\exp(i\tilde{H}t)|\psi_0\rangle} \\ &= -\langle x(-t)\rangle_{\tilde{H}}, \end{aligned} \tag{7}$$

where we have used condition (d). From condition (c), we conclude that $\overline{\langle x(t)\rangle} = -\overline{\langle x(-t)\rangle}$ and, in particular,

$$\overline{\langle x(+\infty)\rangle} = -\overline{\langle x(-\infty)\rangle}. \tag{8}$$

From Eqs. (3) and (8), we have

$$\overline{\langle x(+\infty)\rangle} = 0, \tag{9}$$

which guarantees that the boomerang effect occurs.

Note that Eq. (8) remains valid if the ensemble of disorder realizations is composed only by the two elements H and $\tilde{H} = PTH(PT)^{-1}$. If H is PT symmetric, then $\tilde{H} = H$, condition (c) is trivially met, and Eq. (8) is valid for each disorder realization. If the model has T symmetry, then $\tilde{H} = (P)H(P)^{-1}$ and condition (c) is equivalent to $(P)\{H\}(P)^{-1} = \{H\}$. If the T-symmetric H has complex eigenenergies, once Eq. (3) can be obtained without averaging over many disorder realizations, a boomerang effect is expected for the single pair of realizations H and $\tilde{H} = (P)H(P)^{-1}$ in the sense that one should obtain Eq. (9) using these two realizations.

We note that in the case of a complex spectrum with localized states, the boomeranglike behavior, in principle, might depend on the system size. This is so because, unlike the case with a real spectrum, the wave packet is allowed to move to positions very far from its origin. If the eigenstate $|\phi_l\rangle$ with the largest value for the imaginary part of its eigenenergy is localized far from the origin, it has an exponentially small overlap c_l with $|\psi_0\rangle$. This means that the wave function will take a longer time to become $|\psi(t)\rangle \approx |\phi_l\rangle$. The more one increases the system size, the longer the wave function may take to reach its final state. Therefore, we cannot guarantee a boomeranglike behavior at finite times if, in the case of a complex spectrum, we take the limit of large systems. Indeed, as will be discussed in the next section, our results suggest that the boomeranglike behavior can only be observed for finite chains.

Interestingly, a similar behavior can be observed in delocalized systems under certain circumstances. If the system size is finite and the spectrum is real, one can obtain the diagonal ensemble for the time average of the center of mass over a large enough time interval. However, the timescale at which the boomeranglike behavior can be observed also grows with system size and, eventually, this behavior disappears in the limit of large systems. The QBE, on the other side, differs from the phenomenon described above in the sense that it does not require temporal average and it is present no matter how large the system is.

As a final comment, we emphasize that AL, the symmetry of the ensemble $\{H\}$, and the symmetry of the initial state are crucial for the observation of the QBE, both in the Hermitian and in non-Hermitian cases that we investigate in this paper. As shown above, Hermiticity is not a strict requirement for the boomerang effect. Moreover, if the Hamiltonian is T symmetric, a weak boomerang effect (which depends on the system size) can still appear in cases with complex eigenenergies. Furthermore, our analytical arguments are valid for any dimensions.

III. MODELS AND NUMERICAL RESULTS

In this section, we shall investigate the QBE in several 1D non-Hermitian lattice models. All considered models can be written in the general form

$$H = \sum_j \left[-J_j^R c_{j+1}^\dagger c_j - J_j^L c_j^\dagger c_{j+1} + \epsilon_j c_j^\dagger c_j \right], \tag{10}$$

where $c_j^\dagger$ (c_j) creates (destroys) a particle on site j, $j = 1, 2, \cdots, N$. J_j^R (J_j^L) characterizes the hopping of the particle to the right (left) site and ϵ_j is the on-site potential. The parameters J_j^R, J_j^L, and ϵ_j may be chosen to be real or complex and may lead to Hermitian or non-Hermitian models, models with T symmetry, PT symmetry, or none of these symmetries. These parameters may be random, pseudorandom, or homogeneous. The simplest case is the Hermitian Anderson model, realized with real hoppings $J_j^R = J_j^L = J$ and real on-site potential ϵ_j randomly sampled from a uniform distribution over the interval $[-W/2, W/2]$. When $W > 0$, all states are localized and the model presents the QBE [56,57].

To investigate the QBE, we initialize the system in a Gaussian wave packet,

$$\psi_0(x_j) = \mathcal{N} \exp\left(-x_j^2/2\sigma^2 + ik_0 x_j\right), \tag{11}$$

where $\mathcal{N}$ is a normalization constant, σ^2 is the variance, k_0 is the initial momentum, and x_j is the position of site j (for

TABLE I. Presence of the quantum boomerang effect as a function of the symmetry and the phase of the system. For each symmetry of the Hamiltonian (T, PT, or none of these) and for each phase of the system (Anderson localized with real spectrum, complex spectrum, or delocalized phase), we show with $\surd$ the presence or with ✗ the absence of the QBE. We also show the models we used to check the emergence of the QBE. In this table, we assume that conditions (c) and (d) are valid. *In the AL phase with complex spectrum of the random hopping model, we find that the boomeranglike effect depends on the system size.

	AL with real spectrum	AL with complex spectrum	Extended phase
T	$\surd$ HN model Random hopping model	$\surd$ *Random hopping model	✗ HN model
PT	$\surd$ PT-AA model	✗ Another PT-AA model [41]	✗ PT-AA model
None	$\surd$ T-broken random hopping	✗ T-broken random hopping HN with complex potential Anderson with gain and loss Random gain and loss	✗ HN with complex potential

simplicity, we consider a unitary lattice parameter $a = 1$). This wave function satisfies condition (d) because $PT|\psi_0\rangle = +|\psi_0\rangle$. Once a model is chosen (e.g., the Anderson model or HN model), we make n_d disorder realizations and propagate the wave packet under the corresponding Hamiltonian for each of the realizations using a standard fourth-order Runge-Kutta method. The calculations are done considering open boundary conditions (OBCs), and typically the size N of the system is large enough so the wave function is negligibly small near the edges for all times considered in the propagation. For non-Hermitian models, the norm of the wave functions might be not unitary after time evolution. Hence, we normalize the wave functions $\psi(x_j, t)$ of each disorder realization at each time t. Finally, we take the average of $|\psi(x_j, t)|^2$ over all the disorder realizations to compute the center of mass $\overline{\langle x(t)\rangle}$, second moment $\overline{\langle x^2(t)\rangle}$, and variance $\overline{\sigma(t)}^2 = \overline{\langle x^2(t)\rangle} - \overline{\langle x(t)\rangle}^2$ [56].

We briefly comment on the phenomenology that we observe in the numerical simulations. When conditions (a)–(d) are met, the QBE is present: The wave packet initially propagates balistically with momentum k_0 and $\overline{\langle x(t)\rangle}$ increases with t up to a time t_U where $\overline{\langle x(t)\rangle}$ makes a U-turn. Then $|\overline{\langle x(t)\rangle}|$ decreases with time and vanishes at the limit $t \to +\infty$. The dependence of the QBE on the symmetry of the Hamiltonian and on the phase of the system is shown schematically in Table I, which also shows the models we used in our simulations. In models without T or PT symmetry, we find that, if the spectrum is complex, $\overline{\langle x(t)\rangle}$ typically presents a local minimum at $t_m > t_U$, and increases again for $t > t_m$. We show in the Appendix the evolution of the variance of the wave packet and the failure of the dynamical relation, Eq. (1), for non-Hermitian models.

A. Models with T symmetry

In this section, we analyze two prototypical non-Hermitian T symmetric models which display QBE. We numerically illustrate this result focusing on the HN model with real on-site disorder and in a non-Hermitian random hopping model.

1. Hatano-Nelson model with real on-site disorder

The standard HN model is a non-Hermitian generalization of the Anderson model [1] and is described by the Hamiltonian Eq. (10) by taking real, nonsymmetric hoppings $J_j^R = J + J_a$, $J_j^L = J - J_a$, where J and J_a are the symmetric and antisymmetric components of the hopping amplitudes, respectively. In the standard HN model, one also considers real on-site potential ϵ_j randomly sampled from a uniform distribution over the interval $[-W/2, W/2]$. In the case of PBCs, this model presents a localization transition which coincides with a topological transition and a real-complex transition. The phase where all states are localized is a topologically trivial phase and all its eigenenergies are real. However, the phase where some of the eigenstates are extended possesses a nontrivial winding number and some eigenenergies are complex. The transition between these two phases may be achieved varying either W/J or J_a/J [26]. With OBCs, which we employ in the present calculations, the real-complex transition and the AL transition do not coincide [26,62,63].

In this model, we denote by $\overline{(\ldots)_>}$ the average over disorder realizations of a given variable [such as $|\psi(x,t)|^2$, $\langle x(t)\rangle$, or $\langle x^2(t)\rangle$] in the case where we have chosen a *positive* value for J_a. In other words, $\overline{(\ldots)_>}$ is the average over the ensemble $\{H\}_>$ of disorder realizations with fixed $J_a = J_0 > 0$. Similarly, $\overline{(\ldots)_<}$ is the average over the ensemble $\{H\}_<$ of disorder realizations with a fixed *negative* value for $J_a = -J_0$. For example, $\overline{\langle x\rangle_>}$ is the average of $\langle x\rangle$ over all the disorder realizations of the on-site potentials once we have chosen a value for W and a *positive* J_a, say $J_a/J = 0.5$.

The HN model is T symmetric. The hopping terms of the Hamiltonian, which can be written in the form $H_0 = \sum_j [\, -J^R c_{j+1}^\dagger c_j \;\; -J^L c_j^\dagger c_{j+1}]$, satisfy $(P)H_0(P)^{-1} = \sum_j [-J^R c_j^\dagger c_{j+1} - J^L c_{j+1}^\dagger c_j] \neq H_0$. This means that if we choose in the Hamiltonian H the hopping to the right larger than the one to the left $J^R > J^L$, which is equivalent to $J_a > 0$, we have that in $(P)H(P)^{-1}$ the hopping to the left is larger than the one to the right, and vice versa. Therefore, $(P)\{H\}_>(P)^{-1} = \{H\}_<$. Hence, the analytical arguments of Sec. II do not predict the QBE in $\overline{\langle x(t)\rangle_>}$ or $\overline{\langle x(t)\rangle_<}$. Instead, we choose a value for $|J_a|$ and consider $\overline{(\ldots)} = [\overline{(\ldots)_>} + \overline{(\ldots)_<}]/2$ as the average over the disorder realizations in $\{H\} = \{H\}_> \cup \{H\}_<$, which satisfy $(P)\{H\}(P)^{-1} = \{H\}$. Then we can expect the QBE in $\overline{\langle x(t)\rangle}$ according to our analytical prediction. Notice that averaging over $\{H\} = \{H\}_> \cup \{H\}_<$ is not equivalent to average over disorder realizations of the

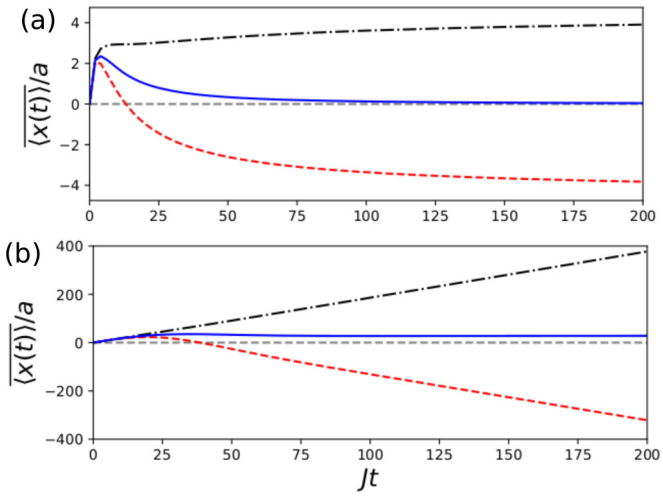

FIG. 1. Quantum boomerang effect in the Hatano-Nelson model. The curves show the disorder-averaged center of mass as a function of time for $|J_a|/J = 0.01$ and (a) $W/J = 3$, where all states are Anderson localized and (b) $W/J = 0.5$, where there are extended states. We used $k_0 a = 1.4$, $\sigma/a = 10$, $N = 5 \times 10^3$ sites and $n_d = 10^6$ disorder realizations. Black dot-dashed (red dashed) lines were obtained with $J_a > 0$ ($J_a < 0$). The blue solid lines were obtained with the average of the two previous lines and show the presence of the QBE in (a) and its absence in (b). The gray dashed lines show the axis $x = 0$. For both panels, the spectrum is real.

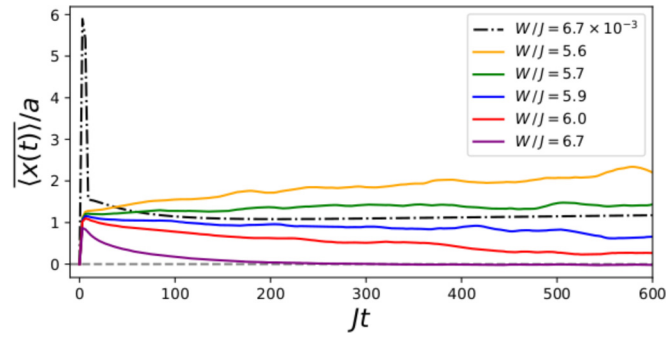

FIG. 2. Probing localization transition using quantum boomerang. Disorder-averaged center of mass $\overline{\langle x\rangle}$ as a function of time in the HN model for $|J_a|/J = 1/3$ and several values of disorder W/J. Here we used $\sigma/a = 10$, $k_0 a = 1.4$, $N = 4 \times 10^3$ sites and $n_d = 10^6$ disorder realizations. The QBE is present for $W/J > W_c/J \approx 5.7$. For all lines with $W/J \geqslant 5.6$, the spectrum is real.

Anderson model, where $J^R = J^L = J$. The resulting DACM $\overline{\langle x(t)\rangle}$ is different in these two models.

Using OBCs, we check numerically that in the localized regime (i.e., $W > W_c$, where W_c is the critical disorder) the spectrum is real and $\lim_{t\to+\infty} \overline{\langle x(t)\rangle}_> = -\lim_{t\to+\infty} \overline{\langle x(t)\rangle}_< \neq 0$. Therefore, for any initial momentum k_0 we find $\lim_{t\to+\infty} \overline{\langle x(t)\rangle} = 0$ and the QBE is present in $\overline{\langle x(t)\rangle}$ but not in $\overline{\langle x(t)\rangle}_{\lessgtr}$, see Fig. 1(a). We note that using a small magnitude of asymmetry of the hoppings $|J_a|/J$ may already lead to a relatively large value of $\lim_{t\to+\infty} \overline{\langle x(t)\rangle}_{\lessgtr}/a$. Further increasing $|J_a|/J$ and keeping W/J fixed causes $\lim_{t\to+\infty} \overline{\langle x(t)\rangle}_{\lessgtr}$ to be even larger. For large enough values of $|J_a|/J$, some of the eigenstates of the Hamiltonian will become extended. This transition can also be reached by fixing $|J_a|/J$ while decreasing W/J. In this regime with extended eigenstates we observe a linear behavior for the DACM at large times, i.e., for $1 \ll Jt$ we have $\overline{\langle x(t)\rangle}_{\lessgtr} \sim bt$, with $b \lessgtr 0$ [see Fig 1(b)]. In this phase, we have $\lim_{t\to\infty} \overline{\langle x(t)\rangle} \neq 0$ and the QBE is not present. In Fig. 2, we investigate the extended-localized transition and its influence on the QBE. Here, to compare our results with the transition found in Ref. [26], we use $|J_a|/J = 1/3$. For PBCs, the transition takes place at $W_c/J \approx 5.7$ [26]. It can be clearly seen in Fig. 2 that for $W < W_c$ we have $\lim_{t\to\infty} \overline{\langle x(t)\rangle} > 0$ and the QBE is absent. For $W > W_c$, there is a U-turn and we have $\lim_{t\to\infty} \overline{\langle x(t)\rangle} = 0$ in agreement with the QBE. Importantly, as in the Hermitian case, the appearance of this effect can be used to find the critical disorder W_c of the model [56].

Here we have shown the presence of the QBE in the HN model when all the states are localized. An additional discussion on the numerical results in this model can be found in Appendix A. We also verify that in the localized regime the variance $\overline{\sigma(t)}$ saturates as $t \to +\infty$ and the dynamical relation, Eq. (1), is a reasonable approximation only if the non-Hermiticity is small, i.e., $|J_a|/J \ll 1$ (see Appendix B). In the following, we investigate another non-Hermitian model with T symmetry.

2. Random hopping model

Reference [57] considered a band random matrix model, which is a Hermitian, T-symmetric model that presents the QBE. The authors considered random hopping amplitudes between the first l neighbors. The model with random hoppings up to first neighbors can be obtained from Eq. (10) by considering real parameters $J_j^R = J_j^L = J + h_j$, where h_j are random numbers sampled from a uniform distribution over $[-W_b/2, W_b/2]$. The on-site potentials ϵ_j are randomly sampled from a uniform distribution over $[-W/2, W/2]$. It was shown in Ref. [57] that one has to consider $J \neq 0$ to be able to observe the QBE, otherwise $\overline{\langle x(t)\rangle}$ is negligibly small at all t. It was also shown that the amplitude of the boomerang $\overline{\langle x(t_U)\rangle}$ decreases when one increases W_b. Here we consider a modification of that model that leads to a non-Hermitian, T-symmetric random hopping model. This is done considering independent hoppings to the right and left, $J_j^R = J + h_j^R$, $J_j^L = J + h_j^L$, where h_j^R and h_j^L are uncorrelated random numbers sampled from a uniform distribution over $[-W_b/2, W_b/2]$. This model meets condition (c). Using $W/J = 2$ and $W_b/J = 1$, we find that the system is in a phase where the states are localized, all eigenenergies are real and the QBE is present (see Fig. 3). As expected, in this localized phase the variance $\overline{\sigma(t)}$ saturates as $t \to +\infty$. We also find that the dynamical relation breaks down in the non-Hermitian random hopping model (see Appendix B).

We verify that, increasing W_b, initially causes the amplitude of the center of mass at the U-turn $\overline{\langle x(t_U)\rangle}$ to decrease. This is in agreement with Ref. [57] in the Hermitian random hopping model, in which the localization length decreases as one increases W_b or W. However, we find that in our non-Hermitian model, increasing W_b beyond a critical value

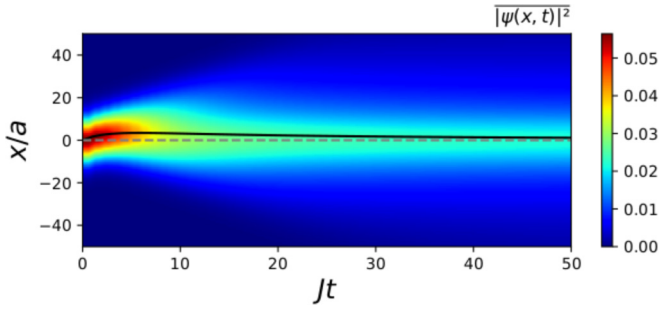

FIG. 3. Boomerang effect in the T-symmetric non-Hermitian random hopping model. Using $W/J = 2$ and $W_b/J = 1$, which correspond to a phase with real eigenenergies, we show a density plot of the disorder-averaged probability distribution. Black solid line shows its center of mass as a function of time and gray dashed line shows the axis $x = 0$. We used $\sigma/a = 10$, $k_0 a = 1.4$, $N = 2 \times 10^3$, and $n_d = 10^6$.

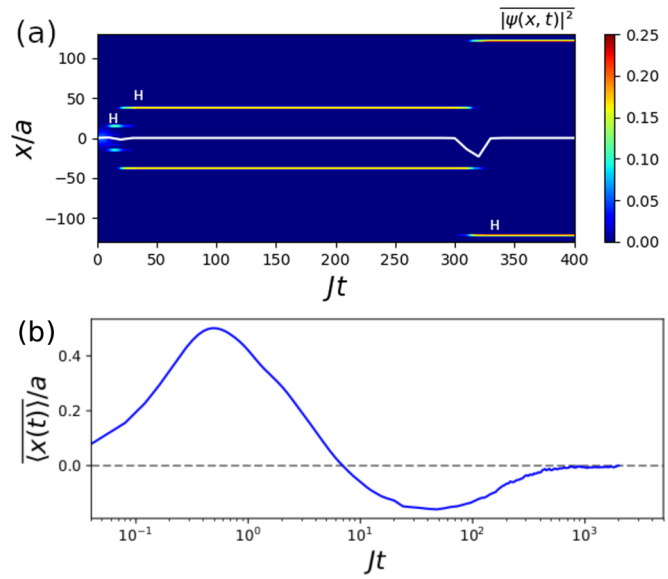

FIG. 4. Boomerang in the non-Hermitian random hopping model with complex spectrum. Using $W/J = 10$, $W_b/J = 3$, $\sigma/a = 10$, $k_0 a = \pi/2$, and $N = 301$, we show in (a) the probability distribution averaged over two disorder realizations, H and its parity-inversion $(P)H(P)^{-1}$. The wave functions are localized in space. The label H in the figure indicates the contribution of the probability distribution that comes from the disorder realization H, while the parity inverted contributions of the figure come from $(P)H(P)^{-1}$. At large times t, the wave functions reach the eigenstates whose eigenenergies have the largest values for their imaginary parts. The disorder averaged center of mass $\overline{\langle x(t)\rangle}$ of these two realizations is given in white curve and vanishes at large times. (b) shows the disorder averaged center of mass of $n_d = 10^6$ realizations and their corresponding parity inversions. Even in this case with complex spectrum, the boomerang behavior is present.

$W_b/J = 2$ causes the appearance of complex eigenenergies, while the states remain localized. The emergence of complex eigenenergies can be understood considering the simple case of a two-site model. In this case, the Hamiltonian can be written as

$$H = \begin{pmatrix} \epsilon_1 & -J - h^L \\ -J - h^R & \epsilon_2 \end{pmatrix}, \tag{12}$$

and we find its corresponding eigenenergies to be $E_\pm = \frac{1}{2}[\epsilon_1 + \epsilon_2 \pm \sqrt{(\epsilon_1 - \epsilon_2)^2 + 4(J + h^L)(J + h^R)}]$. When $W_b/J < 2$, there cannot be complex eigenvalues. When $W_b/J > 2$, there will be complex eigenvalues for some of the realizations of the random parameters ϵ_1, ϵ_2, h^L, h^R.

In our analytical demonstration of the boomerang effect, we required all eigenenergies to be real, except in the case of T-symmetric models [condition (b)], such as the random hopping model we are studying here. Once the eigenstates are localized in this phase, a boomeranglike behavior is expected, even in the case of complex spectrum. In Fig. 4, we show a detailed investigation with evidence of the boomerang behavior. Figure 4(a) illustrates that the wave function tends to be localized in states whose eigenenergies have large imaginary parts ε''. It also shows that the DACM of two disorder realizations H and $(P)H(P)^{-1}$ is essentially zero, except for short intervals when the wave function is migrating to eigenstates with larger ε''. For large enough times, the DACM will remain equal to zero. In Fig. 4(b), we see in the case of many disorder realizations that the DACM tends to vanish for large t, indicating the presence of the boomerang behavior even in the case of complex spectrum, once the model is T symmetric. As mentioned in Sec. II, this behavior was expected for the case of complex spectrum with finite system size and long enough times. In Fig. 4, to see this boomeranglike behavior, we consider a smaller lattice and only observe the boomerang at long times. As we increase the size of the chain, we observe that the DACM tends to saturate at a finite position for the timescale we can numerically compute, being expected to vanish only for much larger times. This indicates that the boomerang behavior disappears in the limit of large system sizes, contrary to the conventional QBE that takes place in the case with a real spectrum.

B. Models with PT symmetry

In this subsection, we shall investigate the presence of the QBE in a non-Hermitian, PT symmetric generalization of the AA model. To that aim, we first demonstrate the QBE in the Hermitian AA model. Next we show results for its non-Hermitian generalization.

1. Hermitian Aubry-André model

In Ref. [57], the authors investigated the QBE in a Hermitian model with real hoppings $J_j^R = J_j^L = J$ and pseudorandom onsite potentials of the form

$$\epsilon_j = W \cos\left(\pi\sqrt{5} j^\gamma\right), \tag{13}$$

where $j > 0$, $\gamma > 0$ and $W > 0$ is the strength of the disorder. The localization of the eigenstates and the presence of QBE depends on the parameter γ. If $\gamma \geqslant 2$, all states are localized and the QBE is present in a very similar way of the Anderson model. For $1 < \gamma < 2$, the state at the band center is delocalized while the other states are localized with a longer localization length. In this case, the QBE is still present, but

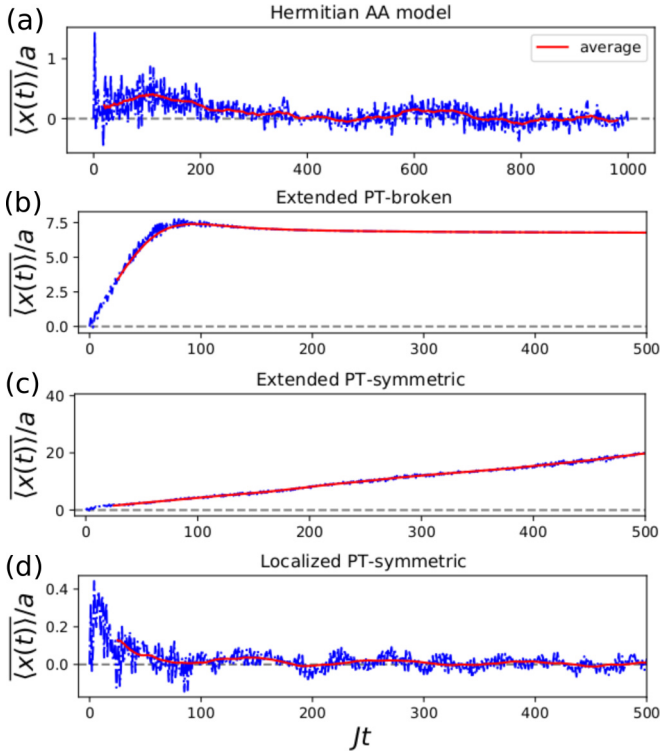

FIG. 5. Boomerang effect in *PT*-symmetric models. The blue dot-dashed lines show $\overline{\langle x(t)\rangle}$. In (a), we consider the Hermitian Aubry-André model and we use $W/J = 2.1$, $k_0 a = 1.4$, $\sigma/a = 1$, $n_d = 10^5$, and $N = 10^3$. The red solid line shows the average of $\overline{\langle x(t)\rangle}$ over the interval $[t - 20/J, t + 20/J]$. In panels (b)–(d), we consider the non-Hermitian *PT*-symmetric Aubry-André model. Here we use $\gamma_0/J = \tan(\pi/3) \approx 1.73$, $k_0 a = \pi/2$, $\sigma/a = 1$, $n_d = 10^5$, $M = 2584$, and $N = 4181$. These panels were obtained with (b) $W/J = 1.6$ and correspond to the *PT* broken phase with extended states; (c) $W/J = 1.8$ and corresponds to the *PT* symmetric phase with extended states; (d) $W/J = 2.2$ and corresponds to the *PT* symmetric phase with localized states, which presents the QBE. The red lines in (b)–(d) show the average of $\overline{\langle x(t)\rangle}$ over the interval $[t - 12.5/J, t + 12.5/J]$.

its height and width depend on the position of the chain where the center of the wave packed is initially located. This may be due to the fact that in this regime the on-site potential has a slowly varying period for large values of the site index j. For $\gamma = 1$, one has the AA model, which possesses a mobility edge at $W_c/J = 2$. For $W < W_c$ ($W > W_c$), all eigenstates of the model are extended (localized). The presence of the QBE was not reported in this model. For $0 < \gamma < 1$, there are extended states and hence the QBE is not expected [57]. Here we report the presence of the QBE in the Hermitian AA model. To mimic the average over disorder realizations, we consider n_d chains, obtained from a shift in the on-site potential ϵ_j. The on-site potential for the ith chain is of the form $\epsilon_j^{(i)} = W \cos[\pi\sqrt{5}(j + i - 1)]$. Figure 5(a) shows $\overline{\langle x(t)\rangle}$ in the Hermitian AA model with $W/J = 2.1 > W_c/J$ and $n_d = 10^5$ realizations. We observe an initial peak $\overline{\langle x(t_U)\rangle} \approx 1.4\,a$ followed by oscillations about an average (in red solid line) that goes to zero as $t \to +\infty$. These fluctuations in the QBE in the AA model are similar to the fluctuations in the QBE in the quantum kicked rotor, both in theory [57] and experiment [58]. In both models, AA and quantum kicked rotor, one has psudorandom potentials. In the case of the AA model, the potential is of the form $\epsilon_j \sim \cos(\beta j + \varphi)$, while in the case of the kicked rotor it is of the form $\epsilon_p \sim \tan(\beta p^2 + \varphi)$ in momentum space [57,64]. One possible cause for the oscillations in both models is the pseudorandom nature of the on-site potentials.

In the AA model, the variance saturates as $t \to +\infty$. On the one side, the standard AA model is Hermitian and the dynamical relation is expected to hold. On the other side, the large amount of fluctuations with time in this model could spoil the computation of the time derivative in Eq. (1). We find, however, that the dynamical relation works reasonably well in this model (see Appendix B). Using $W < W_c$ we do not find the QBE in the AA model due to the presence of extended states in this regime.

2. *Non-Hermitian Aubry-André model with PT symmetry*

Now we investigate the QBE in a non-Hermitian, *PT* -symmetric generalization of the AA model. One such model, discussed in Ref. [31], may be obtained from Eq. (10) choosing complex and asymmetric hoppings $J_j^R = J_{j-1}^L = J_j = J + i\gamma_0 \sin(2\pi\beta j + \varphi) \neq J_{j+1}^*$. The on-site potentials are real, $\epsilon_j = 2W \cos(2\pi\beta j + \varphi)$. Here, γ_0 controls the non-Hermiticity, W is the quasidisorder strength, and $\beta = M/N$, where M and N are two adjacent Fibonacci numbers. One recovers the Hermitian AA model when $\gamma_0 = 0$. It was proved that this Hamiltonian is *PT* symmetric when $\varphi = m\pi/N$ if m is odd (integer) and N is even (odd). It was also shown that depending on the values of J/W and γ_0/W this model may lead to three distinct phases: *PT* broken phase, i.e., with complex eigenenergies, with extended states (for $\gamma_0/W > 1$); *PT* symmetric phase, i.e., with real eigenenergies, with extended states [for $\gamma_0/W < 1$ and $(\gamma_0/W)^2 + (J/W)^2 > 1$]; and *PT* symmetric phase with localized states [for $(\gamma_0/W)^2 + (J/W)^2 < 1$] [31].

In Figs. 5(b)–5(d), we investigate the behavior of the center of mass $\overline{\langle x(t)\rangle}$ in the three phases of the model. It is interesting to note that each of the three phases presents a different behavior for $\overline{\langle x(t)\rangle}$, and the observation of the DACM could be used to find the transition between any of these phases. As expected, the QBE does not appear in the phases with extended states. However, the QBE does appear in the *PT* symmetric phase with localized states. It displays fluctuations similar to the ones that appear in the Hermitian AA model, probably due to the pseudorandom nature of the on-site potentials. The variance also presents a different behavior in each of the three phases (see Appendix B). We find that the dynamical relation breaks down in the phase that presents the QBE.

C. Models without T or PT symmetry

In the following, we illustrate several non-Hermitian models without T or *PT* symmetry and show that the QBE appears only if conditions (a)–(d) are met.

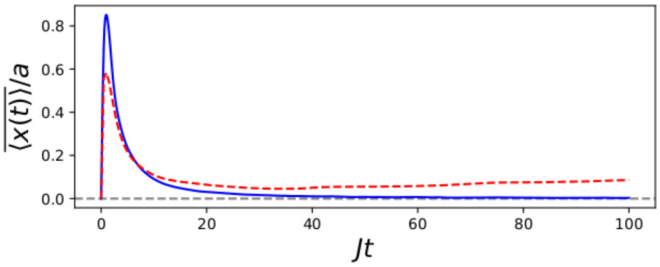

FIG. 6. T-broken random hopping model. We compute $\overline{\langle x(t)\rangle}$ using $W/J = 6$, $k_0 a = 1.4$, $\sigma/a = 10$. In the blue solid line, we use $W_b/J = 1$, $N = 2 \times 10^2$ and $n_d = 10^6$, the spectrum is real and the model presents the QBE. In the red dashed line, we use $W_b/J = 4$, $N = 5 \times 10^2$ and $n_d = 10^7$, the spectrum is complex and the QBE is absent.

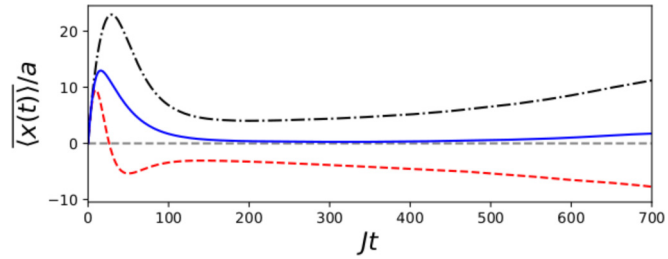

FIG. 7. Hatano-Nelson model with complex potential. We compute $\overline{\langle x(t)\rangle}_>$ (black dot-dashed), $\overline{\langle x(t)\rangle}_<$ (red dashed), and $\overline{\langle x(t)\rangle}$ (blue solid line) using $|J_a|/J = 0.01$, $W/J = 0.5$, $k_0 a = 1.4$, $\sigma/a = 10$, $N = 2 \times 10^3$, and $n_d = 5 \times 10^5$. The model does not present the QBE.

1. T-broken non-Hermitian random hopping model

Here we consider a modification of the random hopping model of Sec. III A 2 that leads to a non-Hermitian, T-broken random hopping model. This is done considering in Eq. (10) independent hoppings to the right and left, $J_j^R = (J + h_j^R)e^{i\phi_j}$, $J_j^L = (J + h_j^L)e^{-i\phi_j}$, where h_j^R and h_j^L are uncorrelated random numbers sampled from a uniform distribution over $[-W_b/2, W_b/2]$ and ϕ_j are sampled uniformly from the interval $[0, \Phi]$, $\Phi > 0$. Time-reversal symmetry is broken due to the random phases ϕ_j and the model is non-Hermitian because $h_j^R \neq h_j^L$ for $W_b > 0$. The on-site potentials ϵ_j are randomly sampled from a uniform distribution over $[-W/2, W/2]$. We find that for $\Phi = 2\pi$, the DACM is negligibly small, in agreement with the Hermitian case with $J = 0$ [57]. Therefore, we use here $\Phi = 1$, once the DACM is finite in this case. We verify that the spectrum is real for $W_b/J < 2$ and complex for $W_b/J > 2$, exactly as was found in the T-symmetric case of Sec. III A 2. The QBE is present in the case of real spectrum because conditions (a)–(d) are met (see Fig. 6). In this case, the variance $\overline{\sigma(t)}$ saturates as $t \to +\infty$. For a complex spectrum, the QBE is absent. This shows the importance of condition (b). In the case of a complex spectrum, $\overline{\langle x(t)\rangle}$ makes the standard U-turn and after that it presents a local minimum at $t = t_m > t_U$, after which it increases again. This local minimum after the U-turn also appears in other non-Hermitian models with complex spectrum and without T and PT symmetry, as we discuss in the following.

2. Hatano-Nelson model with complex potential

In the standard HN model, it was considered in Eq. (10) nonsymmetric hoppings $J_j^R = J + J_a$, $J_j^L = J - J_a$, while the on-site potentials ϵ_j were chosen to be random real numbers. To break T symmetry in that model, here we consider complex on-site potentials $\epsilon_j = |\epsilon_j| e^{i\phi_j}$, where $|\epsilon_j| \in [0, W]$ and $\phi_j \in [0, 2\pi]$ are random numbers with uniform distribution. This model, similarly to the standard HN model, possesses a localization transition. However, in contrast with the standard HN model, the present model with complex on-site potential has complex eigenenergies even in the localized regime, both for OBCs and PBCs [26]. In this model, we consider the ensemble of realizations given by $\{H\} = \{H\}_> \cup \{H\}_<$, as was done in the case of the standard HN model, to ensure that condition (c) is met. In Fig. 7, we show the DACM using parameters in the localized regime and verify that it does not present the QBE once condition (b) is not met. Instead, the DACM presents a local minimum at $t = t_m > t_U$.

3. Anderson model with alternating gain and loss

Now we consider the standard Anderson model [57] with the addition of a gain and loss parameter ($\pm i\gamma$), which alternates from site to site. This Anderson model with alternating gain and loss is obtained from the Hamiltonian Eq. (10) by choosing real hoppings $J_j^R = J_j^L = J$ and complex on-site potential $\epsilon_j = \mathrm{Re}(\epsilon_j) - i\gamma(-1)^j$, where γ is a real parameter that controls the non-Hermiticity of the model and breaks T symmetry. The disorder is encoded in the real part of the on-site potential, $\mathrm{Re}(\epsilon_j)$, which has a uniform distribution over the interval $[-W/2, W/2]$ [27].

The model has complex spectrum and condition (b) is not met. Therefore, we found that the QBE is not present, see Fig. 8(a). As one decreases the value of γ, the asymptotic value of $\overline{\langle x(t)\rangle}$ at long times decreases and the QBE is recovered when $\gamma = 0$. For $\gamma \neq 0$, the DACM presents a U-turn and, after that, $\overline{\langle x(t)\rangle}$ acquires a local minimum value after which it slowly grows.

4. Random gain and loss model

We consider here one more model without T or PT symmetry. In Eq. (10), we choose real hoppings $J_j^R = J_j^L = J$ and purely imaginary on-site potentials $\epsilon_j = -ih_j$, where h_j are random numbers sampled from a uniform distribution over $[-W/2, W/2]$. Figure 8(b) shows that the QBE is not present in this random gain and loss model, which also presents a local minimum in $\overline{\langle x(t)\rangle}$ at $t_m > t_U$.

IV. DISCUSSION AND CONCLUSION

The QBE has been predicted to take place in several Hermitian models with AL and very recently has been experimentally observed in the quantum kicked rotor model. QBE predicts that the DACM of a particle launched with an initial velocity will initially move ballistically, make a U-turn, return to the origin and stop there.

In this paper, we investigated the emergence of the QBE in non-Hermitian systems and clarified the importance of symmetries in the Hamiltonian and in the initial state. We

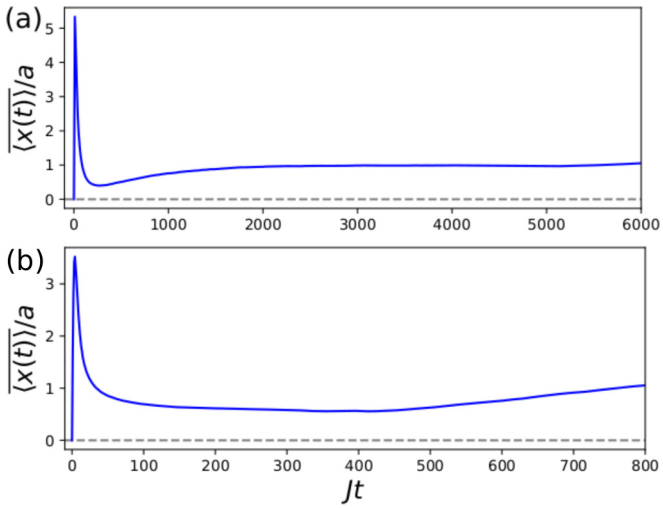

FIG. 8. Center of mass in other models without T or PT symmetry. (a) Anderson model with alternating gain and loss. Here we used $\gamma/J = 0.01$, $W/J = 2$, $k_0 a = 1.4$, $\sigma/a = 10$, $n_d = 10^6$, and $N = 4 \times 10^3$. (b) Random gain and loss model using $W/J = 2$, $k_0 a = 1.4$, $\sigma/a = 10$, $n_d = 10^7$, and $N = 2 \times 10^3$. None of the models present the QBE. In both of them, the center of mass presents a local minimum after the U-turn.

have shown analytically that sufficient conditions to observe a boomerang effect in non-Hermitian systems are: *(a)* AL, (b) reality of the eigenenergies or T symmetry in the case of complex eigenenergies, (c) PT invariance of the ensemble of disorder realizations, and (d) the initial wave function be an eigenstate of the parity-time operator. Our arguments are valid for any dimension.

We confirm our analytical results through a careful numerical investigation of the dynamics in several non-Hermitian models. To study T-symmetric models, we considered the HN model and a non-Hermitian random hopping model. As expected, we confirmed the boomerang effect whenever the eigenstates are localized and all eigenenergies are real. We also verify the boomerang effect when the eigenenergies become complex. However, in this case the boomerang behavior only appears if the system size is finite. We investigated a non-Hermitian PT-symmetric AA model. The dynamics of the DACM and of the variance have a different behavior in each of the three possible phases of the model: extended PT-broken, extended PT-symmetric, and localized PT-symmetric phases. In this last case, the boomerang effect is present, confirming the analytical prediction. We looked for the presence of the QBE in another non-Hermitian PT-symmetric generalization of the AA model, which is known to possess a phase where all states are localized but the eigenenergies are complex (i.e., PT-broken phase) [41]. In this case, the DACM does not return to the origin and the boomerang is absent. This suggests that our analytical arguments cannot be extended to guarantee the QBE in the case of complex eigenenergies in PT-symmetric models. In addition, we investigated a T-broken non-Hermitian random hopping model and found the boomerang in the phase with real spectrum once conditions (a)–(d) are met. This model is more general than all other models presented in the literature about the QBE in the sense that it simultaneously breaks Hermiticity, T symmetry, P symmetry, and PT symmetry. In any of the models with a real spectrum, when the QBE is present we find that the variance saturates with time, as expected. However, the dynamical relation, which relates the center of mass with the time derivative of the second moment, breaks down as we increase non-Hermiticity in the models.

Investigating several non-Hermitian models without T or PT symmetry, we show that the QBE is absent in the case of complex spectrum. We find that all these models present a peculiar behavior: A local minimum of the DACM after the U-turn. This means that the center of mass initially departs from the origin, makes a U-turn toward the origin and, after some time, makes another U-turn, moving away from the origin.

We comment on the experimental implementation of some non-Hermitian models discussed in the paper. Asymmetric hopping amplitudes were proposed for cold atoms in optical lattices in Ref. [26]. Modeling the dynamics via a Lindblad master equation $\dot{\rho}_t = -i[H, \rho_t] + \sum_j \mathcal{D}[L_j]\rho_t$, where $\mathcal{D}[L]\rho \equiv L\rho L^\dagger - \{L^\dagger L, \rho\}/2$, one obtains an effective non-Hermitian Hamiltonian, $H_{\text{eff}} = H - \frac{i}{2}\sum_j L_j^\dagger L_j$ [65] either under postselection or through loss processes in coherent condensates. The effective non-Hermitian Hamiltonian for asymmetric hopping, $H_{\text{eff}} = \sum_j (J_R c_{j+1}^\dagger c_j + J_L c_j^\dagger c_{j+1}) - i\kappa \sum_j c_j^\dagger c_j$, is found by choosing $H = -J\sum_j (c_{j+1}^\dagger c_j + \text{H.c.})$ and the nonlocal jump operators $L_j = \sqrt{\kappa}(c_j \pm i c_{j+1})$ [66]. Nonlocal one-body loss terms L_j can be obtained by adiabatically eliminating a fast-decaying internal excited state in a (anti)magic wavelength in alkaline earth atoms [26,67].

This paper opens possibilities for future investigations in AL systems. For example, we show that the absence of the boomerang effect can be used to find transitions to phases with extended states or to phases with complex eigenenergies. The models studied here may be implemented using cold atoms in optical lattices and the QBE could be experimentally verified in such effective non-Hermitian systems. Future possible investigations include (i) an understanding of why the boomerang effect may present oscillations in some models with pseudodisorder; (ii) a better comprehension of the second return presented in models with complex spectrum; and (iii) a derivation of a generalized dynamical relation valid for non-Hermitian systems. Finally, a relevant open question concerns the fact of whether or not certain interactions preserve the QBE. Specifically, more sophisticated numerical methods can be used to investigate the presence of the quantum boomerang effect in the context of many-body localized phases.

ACKNOWLEDGMENTS

We acknowledge P. Vignolo and L. Tessieri for useful feedback on the paper and A. Moustaj, D. P. Pires, and C. Gao for helpful discussions. We thank the High-Performance Computing Center (NPAD) at UFRN for providing computational resources. T.M. acknowledges the hospitality of ITAMP-Harvard where part of this work was done. T.M. acknowledges CNPq and CAPES for support. T.M. and F.N. acknowledge support from CAPES. This work was supported by the Serrapilheira Institute (Grant No. Serra-1812-27802).

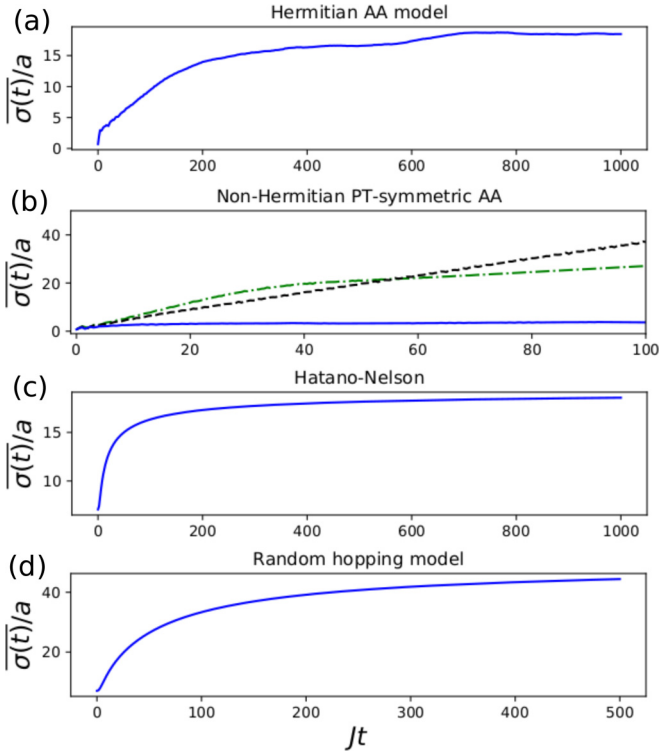

FIG. 9. Variance $\overline{\sigma(t)}$. (a) Hermitian Aubry-André model using the same parameters of Fig. 5(a). (b) Non-Hermitian Aubry-André model using the same parameters of Figs. 5(b)–5(d) with $W/J = 1.6$ in green dot-dashed (extended PT-broken phase), $W/J = 1.8$ in black dashed (extended PT-symmetric phase), and $W/J = 2.2$ in blue solid line (localized PT-symmetric phase), respectively. (c) Hatano-Nelson model using the same parameters of Fig. 1(a). (d) T-symmetric non-Hermitian random hopping model using the same parameters of Fig. 3.

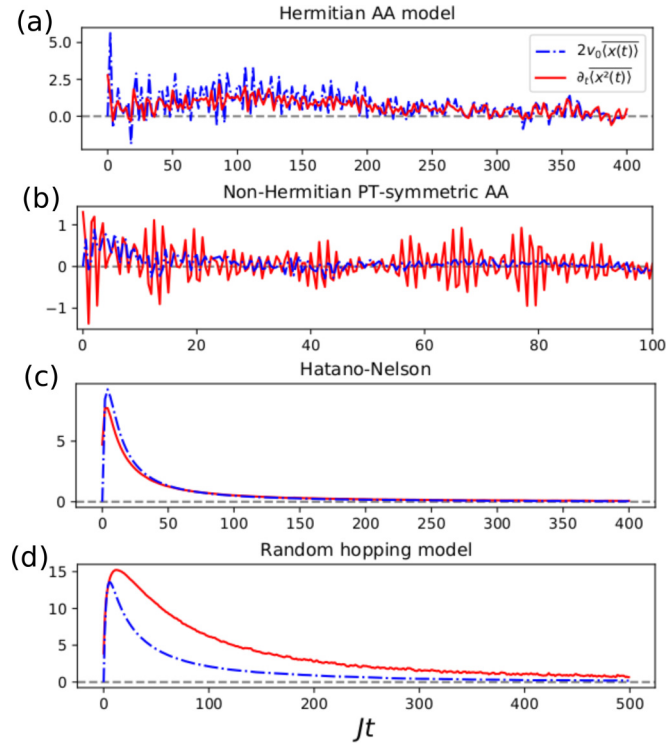

FIG. 10. Breakdown of the dynamical relation. (a) Hermitian Aubry-André model using the same parameters of Fig. 5(a). (b) Non-Hermitian Aubry-André model using the same parameters of Fig. 5(d) (localized PT-symmetric phase). (c) Hatano-Nelson model using the same parameters of Fig. 1(a). (d) Non-Hermitian random hopping model using the same parameters of Fig. 3.

APPENDIX A: DISCUSSION ON THE HATANO-NELSON MODEL

We numerically check that in the standard HN model, if the disorder strength W is such that all the states are localized and if the initial momentum is zero, $k_0 = 0$, then $\overline{\langle x(t)\rangle_>}$ (or $\overline{\langle x(t)\rangle_<}$) is a monotonically nondecreasing (or nonincreasing) function of t that tends to a finite value when $t \to +\infty$. This happens because all the disorder realizations in $\overline{\langle x(t)\rangle_>}$ are such that the hopping to the right is larger than the hopping to the left and, hence, the center of mass have a tendency to move to the right. The reverse is true for $\overline{\langle x(t)\rangle_<}$ and the center of mass tends to move to the left. More generally, for any initial momentum k_0, one has finite values for the center of mass at asymptotically long times, i.e., $\lim_{t\to+\infty}\overline{\langle x(t)\rangle_>} > 0$ and $\lim_{t\to+\infty}\overline{\langle x(t)\rangle_<} < 0$, though for finite k_0 the functions $\overline{\langle x(t)\rangle_{\lessgtr}}$ are not necessarily monotonic functions of the time t and they may present a U-turn in some cases [see Fig. 1(a)]. In the localized phase of the HN model, we find that the asymptotic values $\lim_{t\to+\infty}\overline{\langle x(t)\rangle_{\lessgtr}}$ depend on $|k_0|$, though they do not depend on sign(k_0). The choice of k_0 may also affect the value of $\overline{\langle x(t_U)\rangle_{\lessgtr}}$ and the height of the U-turn $\overline{\langle x(t_U)\rangle}$.

APPENDIX B: VARIANCE SATURATION AND BREAKDOWN OF DYNAMICAL RELATION

Generally speaking, the QBE takes place in AL systems and this localization leads to the absence of diffusion. Therefore, usually the variance of the wave packet is bounded. However, at the critical point W_c of the three-dimensional Anderson model the size of the wave packet increases like $t^{1/3}$ and the QBE still appears [56]. In Fig. 9, we compute the variance using $\overline{\sigma(t)}^2 = \overline{\langle x^2(t)\rangle} - \overline{\langle x(t)\rangle}^2$ for several models considered in this paper that present the QBE, namely, the Hermitian AA model [panel (a)], the localized PT-preserved phase of the non-Hermitian AA model [panel (b)], the HN model [panel (c)], and the T-symmetric random hopping model with real spectrum [panel (d)]. In all these cases, the variance $\overline{\sigma(t)}$ saturates as $t \to +\infty$. This signalizes AL in the investigated models. We also show in FIg. 9(b) the variance in the non-Hermitian AA model in the extended PT-symmetric phase and in the extended PT-broken phase. The variance has a different behavior in each of the three phases of the non-Hermitian PT symmetric AA model.

In Fig. 10, we show the breakdown of the dynamical relation Eq. (1), derived for Hermitian models, where $v_0 = 2Ja\sin(k_0 a)$ is computed from the disorderless model [56,57]. In Fig. 10(a), we consider the standard AA model. As it is a Hermitian model, the dynamical relation holds reasonably well, though there are lots of fluctuations. In Fig. 10(b), the

non-Hermimtian AA model is considered in the localized *PT*-symmetric phase. The agreement between $\partial_t \overline{\langle x^2(t)\rangle}$ and $2v_0\overline{\langle x(t)\rangle}$ is visibly worse in this case. In Fig. 10(c), we consider the HN model with a small non-Hermiticity $|J_a|/J = 0.01$. In this case, the dynamical relation can be a reasonable approximation. However, increasing $|J_a|/J$ leads to the breakdown of the dynamical relation. Figure 10(d) shows the breakdown of that relation for the *T*-symmetric non-Hermitian random hopping model in the phase with real spectrum. We note that no constant factor β could be used to generalize the dynamical relation in the form $\partial_t \overline{\langle x^2(t)\rangle} = 2\beta v_0 \overline{\langle x(t)\rangle}$ for the non-Hermitian models.

[1] P. W. Anderson, Absence of diffusion in certain random lattices, Phys. Rev. **109**, 1492 (1958).

[2] A. A. Chabanov, M. Stoytchev, and A. Z. Genack, Statistical signatures of photon localization, Nature (London) **404**, 850 (2000).

[3] T. Schwartz, G. Bartal, S. Fishman, and M. Segev, Transport and Anderson localization in disordered two-dimensional photonic lattices, Nature (London) **446**, 52 (2007).

[4] H. Hu, A. Strybulevych, J. Page, S. E. Skipetrov, and B. A. van Tiggelen, Localization of ultrasound in a three-dimensional elastic network, Nat. Phys. **4**, 945 (2008).

[5] J. Chabé, G. Lemarié, B. Grémaud, D. Delande, P. Szriftgiser, and J. C. Garreau, Experimental Observation of the Anderson Metal-Insulator Transition with Atomic Matter Waves, Phys. Rev. Lett. **101**, 255702 (2008).

[6] I. Manai, J.-F. Clément, R. Chicireanu, C. Hainaut, J. C. Garreau, P. Szriftgiser, and D. Delande, Experimental Observation of Two-Dimensional Anderson Localization with the Atomic Kicked Rotor, Phys. Rev. Lett. **115**, 240603 (2015).

[7] J. Billy, V. Josse, Z. Zuo, A. Bernard, B. Hambrecht, P. Lugan, D. Clément, L. Sanchez-Palencia, P. Bouyer, and A. Aspect, Direct observation of Anderson localization of matter waves in a controlled disorder, Nature (London) **453**, 891 (2008).

[8] F. Jendrzejewski, A. Bernard, K. Mueller, P. Cheinet, V. Josse, M. Piraud, L. Pezzé, L. Sanchez-Palencia, A. Aspect, and P. Bouyer, Three-dimensional localization of ultracold atoms in an optical disordered potential, Nat. Phys. **8**, 398 (2012).

[9] G. Semeghini, M. Landini, P. Castilho, S. Roy, G. Spagnolli, A. Trenkwalder, M. Fattori, M. Inguscio, and G. Modugno, Measurement of the mobility edge for 3D Anderson localization, Nat. Phys. **11**, 554 (2015).

[10] N. Hatano and D. R. Nelson, Localization Transitions in Non-Hermitian Quantum Mechanics, Phys. Rev. Lett. **77**, 570 (1996).

[11] N. Hatano and D. R. Nelson, Vortex pinning and non-Hermitian quantum mechanics, Phys. Rev. B **56**, 8651 (1997).

[12] N. Hatano and D. R. Nelson, Non-Hermitian delocalization and eigenfunctions, Phys. Rev. B **58**, 8384 (1998).

[13] K. B. Efetov, Directed Quantum Chaos, Phys. Rev. Lett. **79**, 491 (1997).

[14] J. Feinberg and A. Zee, Non-Hermitian random matrix theory: Method of Hermitian reduction, Nucl. Phys. B **504**, 579 (1997).

[15] J. Feinberg and A. Zee, Non-Hermitian localization and delocalization, Phys. Rev. E **59**, 6433 (1999).

[16] P. W. Brouwer, P. G. Silvestrov, and C. W. J. Beenakker, Theory of directed localization in one dimension, Phys. Rev. B **56**, R4333 (1997).

[17] I. Y. Goldsheid and B. A. Khoruzhenko, Distribution of Eigenvalues in Non-Hermitian Anderson Models, Phys. Rev. Lett. **80**, 2897 (1998).

[18] D. R. Nelson and N. M. Shnerb, Non-Hermitian localization and population biology, Phys. Rev. E **58**, 1383 (1998).

[19] A. Amir, N. Hatano, and D. R. Nelson, Non-Hermitian localization in biological networks, Phys. Rev. E **93**, 042310 (2016).

[20] C. Mudry, B. D. Simons, and A. Altland, Random Dirac Fermions and Non-Hermitian Quantum Mechanics, Phys. Rev. Lett. **80**, 4257 (1998).

[21] T. Fukui and N. Kawakami, Breakdown of the Mott insulator: Exact solution of an asymmetric Hubbard model, Phys. Rev. B **58**, 16051 (1998).

[22] I. V. Yurkevich and I. V. Lerner, Delocalization in an Open One-Dimensional Chain in an Imaginary Vector Potential, Phys. Rev. Lett. **82**, 5080 (1999).

[23] S. Longhi, D. Gatti, and G. D. Valle, Robust light transport in non-Hermitian photonic lattices, Sci. Rep. **5**, 13376 (2015).

[24] Q.-B. Zeng, S. Chen, and R. Lü, Anderson localization in the non-Hermitian Aubry-André-Harper model with physical gain and loss, Phys. Rev. A **95**, 062118 (2017).

[25] A. McDonald, T. Pereg-Barnea, and A. A. Clerk, Phase-Dependent Chiral Transport and Effective Non-Hermitian Dynamics in a Bosonic Kitaev-Majorana Chain, Phys. Rev. X **8**, 041031 (2018).

[26] Z. Gong, Y. Ashida, K. Kawabata, K. Takasan, S. Higashikawa, and M. Ueda, Topological Phases of Non-Hermitian Systems, Phys. Rev. X **8**, 031079 (2018).

[27] R. Hamazaki, K. Kawabata, and M. Ueda, Non-Hermitian Many-Body Localization, Phys. Rev. Lett. **123**, 090603 (2019).

[28] H. Jiang, L.-J. Lang, C. Yang, S.-L. Zhu, and S. Chen, Interplay of non-Hermitian skin effects and Anderson localization in nonreciprocal quasiperiodic lattices, Phys. Rev. B **100**, 054301 (2019).

[29] Q.-B. Zeng, Y.-B. Yang, and Y. Xu, Topological phases in non-Hermitian Aubry-André-Harper models, Phys. Rev. B **101**, 020201(R) (2020).

[30] K. Kawabata and S. Ryu, Nonunitary Scaling Theory of Non-Hermitian Localization, Phys. Rev. Lett. **126**, 166801 (2021).

[31] S. Schiffer, X.-J. Liu, H. Hu, and J. Wang, Anderson localization transition in a robust *PT*-symmetric phase of a generalized Aubry-André model, Phys. Rev. A **103**, L011302 (2021).

[32] V. Freilikher, M. Pustilnik, and I. Yurkevich, Effect of Absorption on the Wave Transport in the Strong Localization Regime, Phys. Rev. Lett. **73**, 810 (1994).

[33] C. W. J. Beenakker, J. C. J. Paasschens, and P. W. Brouwer, Probability of Reflection by a Random Laser, Phys. Rev. Lett. **76**, 1368 (1996).

[34] J. C. J. Paasschens, T. S. Misirpashaev, and C. W. J. Beenakker, Localization of light: Dual symmetry between absorption and amplification, Phys. Rev. B **54**, 11887 (1996).

[35] N. A. Bruce and J. T. Chalker, Multiple scattering in the presence of absorption: A theoretical treatment for quasi one-dimensional systems, J. Phys. A: Math. Gen. **29**, 3761 (1996).

[36] S. Longhi, Topological Phase Transition in Non-Hermitian Quasicrystals, Phys. Rev. Lett. **122**, 237601 (2019).
[37] A. F. Tzortzakakis, K. G. Makris, and E. N. Economou, Non-Hermitian disorder in two-dimensional optical lattices, Phys. Rev. B **101**, 014202 (2020).
[38] Y. Huang and B. I. Shklovskii, Anderson transition in three-dimensional systems with non-Hermitian disorder, Phys. Rev. B **101**, 014204 (2020).
[39] E. Rivet, A. Brandstötter, K. G. Makris, H. Lissek, S. Rotter, and R. Fleury, Constant-pressure sound waves in non-Hermitian disordered media, Nat. Phys. **14**, 942 (2018).
[40] S. Weidemann, M. Kremer, S. Longhi, and A. Szameit, Topological triple phase transition in non-Hermitian Floquet quasicrystals, Nature (London) **601**, 354 (2022).
[41] S. Longhi, Metal-insulator phase transition in a non-Hermitian Aubry-André-Harper model, Phys. Rev. B **100**, 125157 (2019).
[42] C. M. Bender and S. Boettcher, Real Spectra in Non-Hermitian Hamiltonians Having *PT* Symmetry, Phys. Rev. Lett. **80**, 5243 (1998).
[43] C. M. Bender, PT-symmetric quantum theory, J. Phys.: Conf. Ser. **631**, 012002 (2015).
[44] C. M. Bender, P. E. Dorey, C. Dunning, A. Fring, D. W. Hook, H. F. Jones, S. Kuzhel, G. Lévai, and R. Tateo, *PT Symmetry* (World Scientific, Singapore, 2019).
[45] J. A. S. Lourenço, R. L. Eneias, and R. G. Pereira, Kondo effect in a *PT*-symmetric non-Hermitian Hamiltonian, Phys. Rev. B **98**, 085126 (2018).
[46] J. A. S. Lourenço, G. Higgins, C. Zhang, M. Hennrich, and T. Macrì, Non-Hermitian dynamics and *PT*-symmetry breaking in interacting mesoscopic Rydberg platforms, Phys. Rev. A **106**, 023309 (2022).
[47] Y. Pará, G. Palumbo, and T. Macrì, Probing non-Hermitian phase transitions in curved space via quench dynamics, Phys. Rev. B **103**, 155417 (2021).
[48] D. P. Pires and T. Macrì, Probing phase transitions in non-Hermitian systems with multiple quantum coherences, Phys. Rev. B **104**, 155141 (2021).
[49] D. P. Pires and T. Macrì, Entanglement timescale and mixedness in non-Hermitian quantum systems, arXiv:2209.11667.
[50] B. Zhang, Q. Li, X. Zhang, and C. H. Lee, Real non-Hermitian energy spectra without any symmetry, Chin. Phys. B **31**, 070308 (2022).
[51] R. Yang, J. W. Tan, T. Tai, J. M. Koh, L. Li, S. Longhi, and C. H. Lee, Designing non-Hermitian real spectra through electrostatics, arXiv:2201.04153.
[52] S. Longhi, Phase transitions in a non-Hermitian Aubry-André-Harper model, Phys. Rev. B **103**, 054203 (2021).
[53] S. Aubry and G. André, Analyticity breaking and Anderson localization in incommensurate lattices, Ann. Israel Phys. Soc. **3**, 18 (1980).
[54] Y. G. Sinai, Anderson localization for one-dimensional difference Schrödinger operator with quasiperiodic potential, J. Stat. Phys. **46**, 861 (1987).
[55] T. Liu, H. Guo, Y. Pu, and S. Longhi, Generalized Aubry-André self-duality and mobility edges in non-Hermitian quasiperiodic lattices, Phys. Rev. B **102**, 024205 (2020).
[56] T. Prat, D. Delande, and N. Cherroret, Quantum boomeranglike effect of wave packets in random media, Phys. Rev. A **99**, 023629 (2019).
[57] L. Tessieri, Z. Akdeniz, N. Cherroret, D. Delande, and P. Vignolo, Quantum boomerang effect: Beyond the standard Anderson model, Phys. Rev. A **103**, 063316 (2021).
[58] R. Sajjad, J. L. Tanlimco, H. Mas, A. Cao, E. Nolasco-Martinez, E. Q. Simmons, F. L. N. Santos, P. Vignolo, T. Macrì, and D. M. Weld, Observation of the Quantum Boomerang Effect, Phys. Rev. X **12**, 011035 (2022).
[59] J. Janarek, B. Grémaud, J. Zakrzewski, and D. Delande, Quantum boomerang effect in systems without time-reversal symmetry, Phys. Rev. B **105**, L180202 (2022).
[60] F. Noronha and T. Macrì, Ubiquity of the quantum boomerang effect in Hermitian Anderson-localized systems, Phys. Rev. B **106**, L060301 (2022).
[61] For each disorder realization, one has that $\langle x(t)\rangle = \sum_{n\neq m} c_n c_m^* \exp[-i(\epsilon_n-\epsilon_m)t]\langle\phi_m|x|\phi_n\rangle + \sum_n |c_n|^2\langle\phi_n|x|\phi_n\rangle$ presents fluctuations with time due to the off-diagonal terms and they oscillate about a time-independent component given by the diagonal terms. It is assumed that performing the average over disorder realizations at long times causes these time-dependent terms to cancel due to the random phases. We numerically confirm the validity of the diagonal ensemble due to the disorder average.
[62] K. Kawabata, K. Shiozaki, M. Ueda, and M. Sato, Symmetry and Topology in Non-Hermitian Physics, Phys. Rev. X **9**, 041015 (2019).
[63] L. Li, C. H. Lee, and J. Gong, Impurity induced scale-free localization, Commun. Phys. **4**, 42 (2021).
[64] S. Fishman, D. R. Grempel, and R. E. Prange, Chaos, Quantum Recurrences, and Anderson Localization, Phys. Rev. Lett. **49**, 509 (1982).
[65] G. Lindblad, On the generators of quantum dynamical semigroups, Commun. Math. Phys. **48**, 119 (1976).
[66] Z. Gong, S. Higashikawa, and M. Ueda, Zeno Hall Effect, Phys. Rev. Lett. **118**, 200401 (2017).
[67] F. Reiter and A. S. Sørensen, Effective operator formalism for open quantum systems, Phys. Rev. A **85**, 032111 (2012).